Biochemical Pharmacology 80 (2010) 1373–1385

Contents lists available at ScienceDirect

Biochemical Pharmacology

journal homepage: www.elsevier.com/locate/biochempharm

Chain-dependent photocytotoxicity of tricationic porphyrin conjugates and related mechanisms of cell death in proliferating human skin keratinocytes

João Nuno Silva [a,b,c,d], Antoine Galmiche [b,c,d], João P.C. Tomé [e], Agnès Boullier [b,c,d], Maria G.P.M.S. Neves [e], Eduarda M.P. Silva [e], Jean-Claude Capiod [f], José A.S. Cavaleiro [e], René Santus [g], Jean-Claude Mazière [b,c,d], Paulo Filipe [a], Patrice Morlière [b,c,d,*]

[a] Faculdade de Medicina de Lisboa, Hospital de Santa Maria, Clinica Universitária de Dermatologia, Lisboa, Portugal
[b] INSERM, ERI12, Amiens, France
[c] Université de Picardie Jules Verne, Faculté de Médecine et de Pharmacie, EA 4292, Amiens, France
[d] CHU Amiens, Laboratoire de Biochimie, Amiens, France
[e] University of Aveiro, Department of Chemistry, Aveiro, Portugal
[f] CHU Amiens, Laboratoire d'Hématologie, Amiens, France
[g] Muséum National d'Histoire Naturelle, RDDM, Photobiologie, Paris, France

ARTICLE INFO

Article history:
Received 14 June 2010
Accepted 23 July 2010

Keywords:
PDT
Photocytotoxicity
Necrosis
Autophagy
Caspases
MAPK pathway

ABSTRACT

Photodynamic therapy (PDT) is a poor treatment option for nodular basal cell carcinomas and squamous cell carcinomas. As a result, the search for new photosensitizers with better effectiveness is of current interest. The photocytotoxicity of conjugates (P-R) of a water-soluble tri-cationic porphyrin (P-H) having similar efficiency of production of singlet oxygen, the PDT cytotoxin, has been assessed *in vitro*. Links between uptake, intracellular localization, photooxidative stress, photocytotoxicity and ability to induce programmed cell death are established. Conjugates bearing methyl (P-Me), Di-O-isopropylidene-(-D-galactopyranosyl (P-OGal) or *N,N′*-dicyclohexylureidooxycarbonyl (P-DDC) chains are efficiently taken-up by proliferating NCTC 2544 keratinocytes. The relative order of photocytotoxicity is P-OGal >P-DDC = P-Me ≫ P-H. The photocytotoxic potential of P-Me, P-OGal and P-DDC equals that of endogenous protoporphyrin IX induced by δ-aminolevulinic acid or its esters, the pro-drugs currently employed for PDT of skin lesions. Microfluorometry shows that P-Me, P-OGal, and P-DDC localize in endocytotic or pinocytotic vesicles but not in mitochondria or nucleus. Absence of annexin V binding, caspase activation or chromatin condensation suggests that cell photosensitization by P-R does not induce apoptosis. On the other hand, P-OGal photocytotoxicity correlates with appearance of multiple vesicles that have hallmarks of autophagy compartments, being decorated with the marker LC3 in cells transfected with an expression vector encoding GFP-LC3. p38 and JNK phosphorylation and inhibition of ERK1/2 phosphorylation suggest close relationship between mortality of NCTC 2544 keratinocytes and MAPK pathway impairment. Given their potentially easy formulation, water-soluble P-R are promising powerful photosensitizers for PDT of skin lesions.

1. Introduction

The treatment of malignant or benign skin diseases by photodynamic therapy (PDT) has developed rapidly [1]. Current evidence indicates that topical PDT is effective in actinic keratosis, Bowen's disease and basal cell carcinoma (BCC) but it is a relatively poor treatment option for either squamous cell carcinomas or nodular BCC. In current skin PDT, topical application of δ-aminolevulinic acid (ALA) or its methyl ester (MAL), precursors of protoporphyrin IX (PPIX), is followed by illumination of the diseased area with red light. The poor water solubility of these agents requires expensive preparation of formulations for systemic or topical administration. Hence, development of new

Abbreviations: 3-MA, 3-methyladenine; ALA, 5-aminolevulinic acid; A, annexin V-FITC; BCC, Basal cell carcinoma; CHAPS, 3-[(3-cholamidopropyl)dimethylammonio]-1-propanesulfonic acid; EMEM, minimum essential medium with Earle's salts; FCS, fetal calf serum; GFP, Green fluorescent protein; HBSS, Hanks' balanced saline solution; LC3, microtubule-associated protein light-chain 3; MAL, methyl aminolevulinate; NR, neutral red; DPBS, Dulbecco's phosphate-buffered saline; PDT, photodynamic therapy; PI, propidium iodide; PPIX, protoporphyrin IX; ROS, reactive oxygen species; SDS, sodium dodecyl sulfate; TBARS, thiobarbituric acid reactive substances; TX100, triton X100.

* Corresponding author at: INSERM ERI12, Laboratoire de Biochimie, CHU Amiens - Hôpital Nord, place Victor Pauchet, 80054 Amiens Cedex 1, France.
Tel.: +33 3 22 66 86 69; fax: +33 3 22 66 85 93.
E-mail address: morliere.patrice@chu-amiens.fr (P. Morlière).

0006-2952/$ – see front matter © 2010 Elsevier Inc. All rights reserved.
doi:10.1016/j.bcp.2010.07.033

photosensitizers with better effectiveness is of current interest. Such new photoactive substances might demonstrate better clinical and histological efficacy in treating skin lesions for which topical MAL-PDT is ineffective (e.g. melanoma) or might be used as a palliative treatment for patients with plaque-type cutaneous T-cell lymphoma. Despite superior absorbance in the 700 nm region (molar absorptivity: $\sim 2 \times 10^5\ M^{-1}\ cm^{-1}$) phthalocyanines are not currently used in the PDT of epidermal skin lesions (normally ~1–2 mm thickness). They tend to form aggregates of reduced uptake and photosensitizing properties and the phthalocyanine ring resists to biodegradation [2]. However, their encapsulation in silica nanoparticles would appear to provide a promising approach to photosensitizer uptake and delivery as it has already been shown to improve the aqueous solubility and stability of the silicon phthalocynanine 4 [3]. For these reasons, the synthesis of water-soluble derivatives of porphyrins and chlorins has been investigated. Conjugation of amino-acids, peptides and sugars to photosensitizers favours specific targeting since such groups play key roles in the recognition and metabolism in micro-organisms and cells [4,5].

In this study, new water-soluble derivatives of 5-(4-carboxyphenyl)-10,15,20-tris(4-methylpyridinium-4-yl)porphyrin tri-iodide (P-R), whose absorbance maxima are shifted to the red by 15–20 nm as compared to PPIX, have been shown to be of potential interest in dermatological PDT since a poly-S-lysine conjugate is, *in vitro,* an effective photosensitizer towards rapidly proliferating human skin keratinocytes [6]. Furthermore, tricationic porphyrins are promising molecules since they may bind to negatively charged skin cells after disruption of the *Stratum Corneum* barrier. In this study, the photocytotoxicity effectiveness of conjugates with a methyl (P-Me), a dicyclohexylureidooxy group (P-DDC), a di-*O*-isopropylidene-α-D-galactopyranosyl group (P-OGal), a α/β-D-galactopyranosyl group (P-Gal) has been evaluated in cultured proliferating human skin keratinocytes for allowing the direct comparison of results obtained with the poly-*S*-lysine conjugate (P-$(Lys)_n$) [6]. We have also determined the molecular mechanisms involved in the photo-induced cell death, the induction of a specific death mode being susceptible to result in a therapeutic advantage.

2. Materials and methods

2.1. Chemicals, culture media and routine spectroscopic equipment

Reagents for cell culture, minimum essential medium with Earle's salts (EMEM), Hanks' balanced saline solution containing 20 mM Hepes (HBSS), Dulbecco's phosphate-buffered saline (DPBS), all without phenol red, fetal calf serum (FCS), trypsin and antibiotics were purchased from Sigma Chemical Co (St. Louis, MO, USA). Chemicals and reagents were obtained from Sigma chemical Co., Merck (Darmstadt, Germany), Fluka (Saint-Quentin Fallavier, France) and Molecular Probes (Eugene, OR, USA) [6]. Inhibitors of p38 (SB203580) and JNK (SP600125) were purchased from Calbiochem (Darmstadt, Germany). Specific antibodies against caspase-3, caspase-8, caspase-9 and p62/SQSTM1 were provided by Santa Cruz Biotechnology (Heidelberg, Germany) whereas those against total p38, phospho-p38, total JNK, phospho-JNK, total Akt, phospho-Akt, total ERK, phospho-ERK were purchased from Cell Signaling (Beverley, MA, USA). The synthesis of the porphyrin conjugates (P-R) (Fig. 1) was performed as described by Tomé et al. [5,7]. The 500 μM stock solutions were prepared in water:DMSO (1:1, v/v) and stored at 0–4 °C. A UVIKON 943 spectrophotometer from Kontron Instruments (Montigny les Bretonneux, France) was used for optical absorption spectrophotometry. Fluorescence measurements were carried out with a SLM AMINCO-BOWMAN (series 2) fluorometer (Bioritech, Chamarande, France).

2.2. Cell culture and treatment

The immortalized NCTC 2544 human skin keratinocyte cell line was purchased from ICN Flow (Fontenay sous Bois, France). Cells were propagated, grown and seeded as earlier described [6]. For

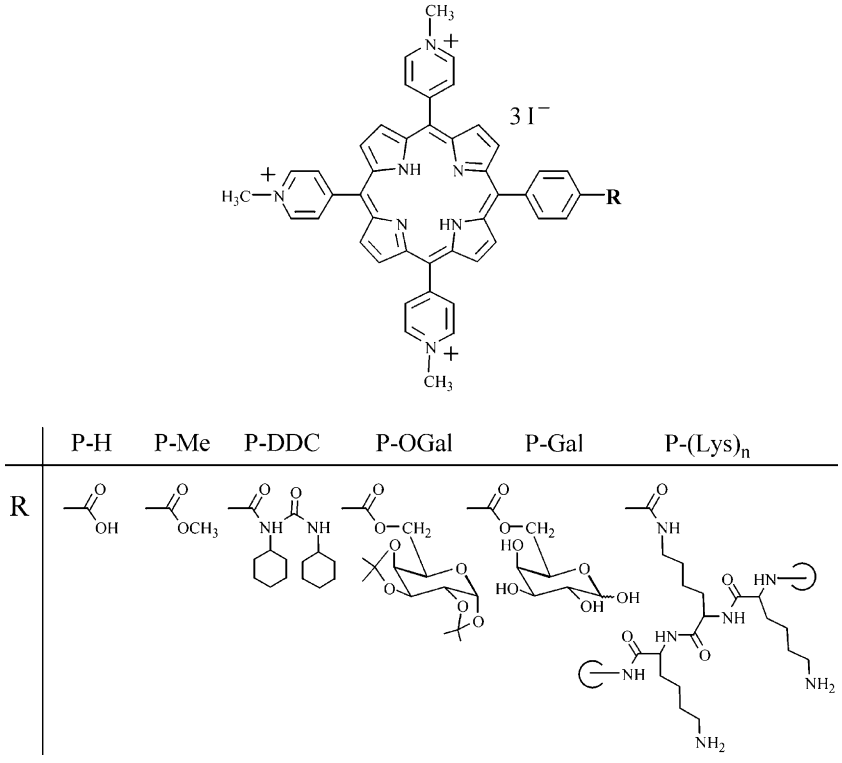

Fig. 1. Chemical structure of P-R derivatives.

fluorescence microscopy, cells were seeded on 30 mm diameter and 0.15 mm thick coverglass at a density of about 1700 cells/cm^2 (2.5 mL at about 5000 cells/mL) and were grown for 4 days. The incubations were carried out with 1 mL of P-R at various concentrations and for various times in either HBSS or 10% FCS-supplemented EMEM. In the case of endogenous PPIX synthesis, incubations were performed with 0.2–0.8 mM ALA in 10% FCS-supplemented EMEM. After incubation, cells were washed twice with 4 mL of HBSS before measurements.

2.3. Irradiation

Washed cell monolayers, covered with 1 mL of HBSS without photosensitizer, were irradiated with broad band red light provided by a custom-built table consisting of two 300 W tungsten-halogen lamps whose light was filtered with Balzers Y54 and calflex 3000 optical filters [6,8]. Petri dishes were placed on a 30 × 25 cm thermostated (37 °C) glass table above the lamps. Under these conditions, most of the light originates from wavelengths in the range 500–750 nm as determined with a CS 1000A Minolta spectroradiometer. The lamp actinometry is described in supplementary data.

2.4. Determination of intracellular photosensitizer concentration

Immediately after P-R or ALA incubation and washings, cells were mechanically scrapped in 1 mL of water. After collection, 100 μL of an 11% SDS solution in 10 mM phosphate buffer (pH 7.0) were added to the disrupted cell suspension. Fifty μL of this solution were saved for protein determination using Lowry's method with Folin reagent. The remainder was utilized for fluorometric measurement of photosensitizer concentration, using standard P-R solutions for calibration (λ_{exc} = 427 nm and λ_{em} = 659 nm) or standard PPIX solutions (λ_{exc} = 407 nm and λ_{em} = 636 nm) [9]. Data are the mean ± SD of at least three independent experiments, each performed in triplicate.

2.5. Neutral Red uptake assay

The assessment of photocytotoxicity by the NR uptake assay has been validated by the European Union for the testing of phototoxic chemicals and for the classification and labelling of hazardous chemical (EU Commission Directive 2000/33/EC). This assay has been fully described by Filipe et al. [10].

2.6. Thiobarbituric acid reactive substances (TBARS) assay

Immediately after irradiation or sham-irradiation, 0.9 mL of supernatants was collected. After addition of 90 μL of butylated hydroxytoluene (2% w/w in ethanol) samples were kept frozen until TBARS assay. Cells were washed twice with DPBS, scrapped and collected for protein determination. TBARS were fluorometrically determined in terms of malondialdehyde equivalent as earlier described [6].

2.7. Fluorescence microscopy equipment for photosensitizer localization

An inverted fluorescence microscope (Eclipse TE 2000 DV Nikon) equipped with a CoolSNAP$_{HQ}$^{TM} detector cooled to −30 °C (Princeton Instruments; Division of Roper Scientific, Evry, France) was used for cell microfluorometry. This system is controlled by the Metaview/Metamorph software, which is also used for image analyses. The fluorescence recording conditions (objective, camera binning and exposure time, dichroic mirrors, filters) are fully described in ref. [6]. No porphyrin fluorescence was detected with the green emission filter while negligible fluorescence of the LysoTracker Green was recorded with the red emission filter. Background fluorescence obtained from cell-free areas was subtracted from all the acquired images.

2.8. Flow cytometry

At various times after photosensitization, adherent cells were washed twice in ice-cold DPBS and detached with Accutase™ (Sigma–Aldrich Co). Cells were transferred to 15 mL conical tubes and gently washed with serum supplemented medium by low speed centrifugation at 1500 rpm for 5 min. Cell pellets were washed once with DPBS and then re-suspended in assay buffer (0.1 M HEPES/NaOH, pH 7.4; 140 mM NaCl; 25 mM $CaCl_2$) at a concentration of 1×10^6 cells/mL. Annexin V-FITC binding was assessed using the Santa Cruz Biotechnology Apoptosis Kit (Santa Cruz Biotechnology, Heidelberg, Germany) according to the manufacturer's protocol. After 15 min of incubation in the dark with annexin V-FITC (5 μg/mL) and propidium iodide (PI) (5 μg/mL), cell fluorescence was measured in the spectral regions 505–545 nm (FL1) for annexin V-FITC (A) and 610–650 nm (FL3) for PI with a Cytomics FC 500 flow cytometer (Beckam Coulter, Villepinte, France). Data analysis was performed using Cytomics Analysis software.

2.9. DNA fragmentation assay

DNA fragmentation was assessed through determining cytoplasmic accumulation of histone-associated DNA fragments by an enzyme-linked immunosorbent assay (Roche Diagnostics, Mannheim, Germany). At different times after irradiation, the cell supernatant was removed, cells were washed twice with ice-cold DPBS and lysed with the kit buffer. Equal amounts of protein from the cytoplasmic fraction (100 μg, Bradford assay from Bio-Rad Laboratories, Marne-la-Coquette, France) were transferred into an anti-DNA precoated microtiter plate and analyzed using the ELISA procedure recommended by the manufacturer.

2.10. Caspase assays

After irradiation cells were lysed in buffer (10 mM HEPES, pH 7.4, 2 mM EDTA, 0.1% CHAPS, 5 mM dithiothreitol and 1 mM phenylmethylsulfonyl fluoride, supplemented with 10 μg/mL pepstatin, aprotinin and leupeptin), sonicated and centrifuged at 14,000 × g for 5 min at 4 °C. Supernatants were saved as representative cytosol extracts. Aminomethylcoumarin (AMC)-conjugated peptide substrates at a final concentration of 20 μM were added to 40 μg of total cytosol protein and incubated for 30 min at 37 °C. The specific substrates used were: acetyl-Asp-Glu-Val-Asp-AMC (Ac-DEVD-AMC) for caspase-3, acetyl-Ile-Glu-Thr-Asp-AMC (Ac-IETD-AMC) for caspase-8 and acetyl-Leu-Glu-His-Asp-AMC (Ac-LEHD-AMC) for caspase-9 (AnaSpec, Inc, San Jose, CA, USA). The fluorescence of coumarin dyes was measured with a 96-microwell plate reader under excitation at 360 nm and emission at 460 nm.

2.11. Immunoblot analysis

Cells were lysed in RIPA buffer supplemented with protease and phosphatase inhibitors. The protein concentration of cell extracts was determined using the Pierce BCA assay (Thermo Fisher Scientific, Cergy Pontoise, France) and equal amounts of proteins (40 μg) were separated by 12% SDS-PAGE and transferred onto nitrocellulose membranes. Membranes were immunoblotted using conventional procedures and revealed using an enhanced chemiluminescence detection kit from Amersham (Saclay, France). Western blots were scanned and quantified using the software ImageJ (National Institutes of Health).

2.12. Cell transfection with GFP-LC3

The construct encoding microtubule-associated-protein-light-chain-3 (LC3) protein tagged at its N-terminus with green fluorescent protein (GFP), GFP-LC3, has been used to monitor autophagy through direct fluorescence microscopy and was provided by Drs. T. Yoshimori and N. Mizshima (Department of Bioregulation and Metabolism, The Tokyo Metropolitan Institute of Medical Science, Japan) [11]. NCTC 2544 cells grown on glass coverslips were transfected with GFP-LC3 using Lipofectamine 2000 according to the supplier's protocol (Invitrogen). After transfection, cells were incubated for 3 h with 5 μM P-OGal or for 18 h with 0.8 mM ALA and irradiated for 15 min. At various times after irradiation, cells were fixed with paraformaldehyde, rinsed and mounted on glass slides using Mowiol (Calbiochem). Cells were observed under a Nikon Eclipe TE2000-U fluorescence microscope equipped with a plan APO VC 60×/1.40 objective under oil immersion. Cells with active autophagy were defined as those displaying 3 or more puncta of GFP-LC3. Results are given under each experimental condition as percentage of cells with more than 3 puncta of GFP-LC3, and are based on the counting of over 500 cells expressing GFP-LC3.

2.13. Cytochrome c immunofluorescent staining

Cells grown on glass coverslips and treated as indicated were washed with PBS, fixed with 4% paraformaldehyde, and permeabilized with 0.1% TX100. Immunolabelling was performed using a mouse antibody raised against cytochrome *c* (BD Bioscience, Le Pont de Claix, France) and a secondary antibody labeled with Cy3 (Jackson Immunoresearch). Nuclei were counterstained with DAPI. The stained samples were rinsed and mounted in Mowiol (Calbiochem) and the slides were examined and photographed using a Nikon Eclipe TE2000-U fluorescence microscope equipped with a plan APO VC 60×/1.40 objective under oil immersion.

2.14. Statistical analyses

Statistical analyses were performed with the Student's *t*-test. Statistical significances are provided in the figures ($^{*}p < 0.05$, $^{**}p < 0.01$).

3. Results

3.1. Uptake of P-R derivatives by cells

NCTC 2544 keratinocytes have been incubated at various durations with increasing concentrations of porphyrins in FCS-supplemented EMEM. As shown in Fig. 2A, the uptake of all derivatives is extremely fast and reaches a plateau within less than an hour. No further uptake is observed with incubation of up to 18 h. P-H and, to a lesser extent, P-Gal are poorly incorporated when compared to P-Me, P-DDC and P-OGal. After a 3 h incubation in FCS-supplemented EMEM, the uptake increases almost linearly

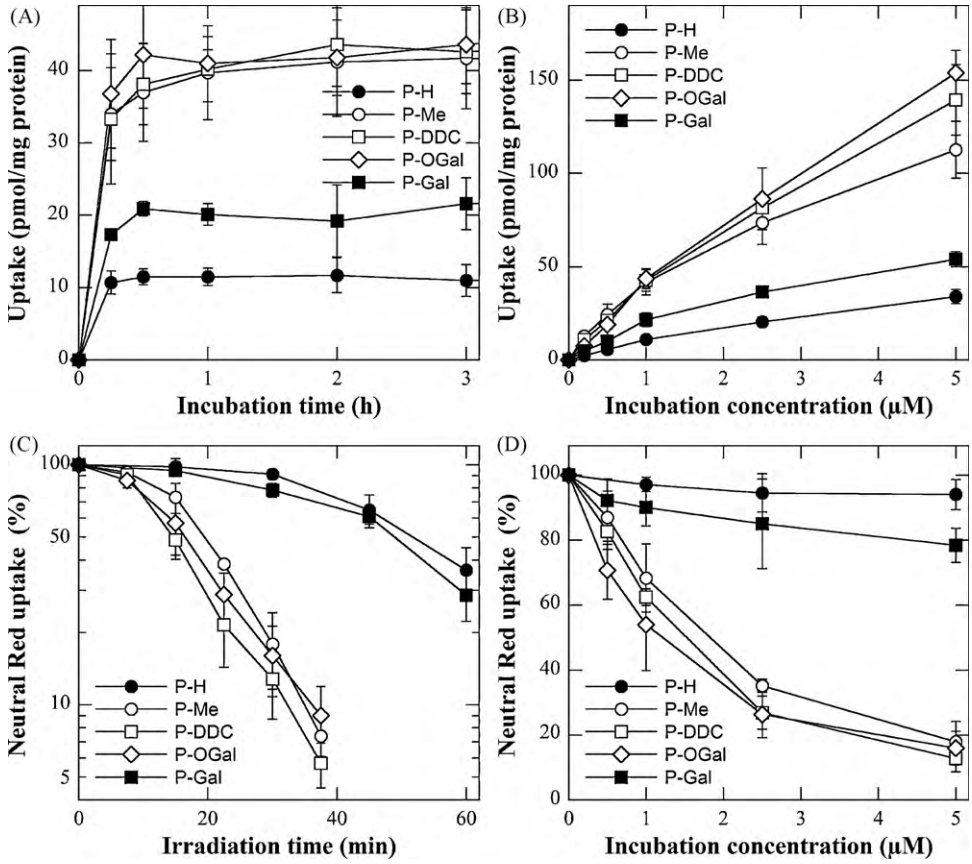

Fig. 2. (A and B) Uptake of P-H, P-Me, P-DDC, P-OGal, P-Gal (●,○,□,◇,■) by NCTC 2544 keratinocytes as a function of the time of incubation with 1 μM P-R (A) and of the P-R concentration during 3 h incubation (B) in FCS-supplemented culture medium. Data are the mean of at least three independent experiments performed in triplicates. (C and D) Cytotoxic effects photosensitized by P-H, P-Me, P-DDC, P-OGal, P-Gal (●,○,□,◇,■) as a function of the irradiation time (C) and of the incubation concentration (D) in FCS-supplemented culture medium. In C, cells were incubated for 3 h with 5 μM P-R prior to irradiation, whereas in D cells were irradiated for 30 min after incubation for 3 with the desired P-R concentration. A 100% Neutral Red (NR) uptake corresponds to sham-irradiated untreated cells. Data are the mean of at least three independent experiments performed in triplicates. Note the logarithmic *Y*-axis in C.

Table 1
Photosensitization of NCTC 2544 keratinocytes by tricationic porphyrins.

	P-H	P-Me	P-DDC	P-OGal	P-Gal	P-(Lys)$_n$[c]
PC_{50} (μM)[a]	>>5	~1.8	~1.5	~1.2	>5	~3.1
IPC_{50} (pmol/mg protein)[b]	>>35	~55	~55	~50	>50	~260
Inhibition by N_3^- (%)[d]	100 ± 7	95 ± 11	88 ± 12	93 ± 12	100 ± 2	–

Photocytotoxic concentration (PC_{50}), intracellular phototoxic content (IPC_{50}) and inhibition of photocytotoxicity by N_3^- ions.
[a] PC_{50} is defined as the incubation concentration necessary to obtain a 50% decrease in NR uptake after a 30 min irradiation. Data were obtained from Fig. 2D.
[b] IPC_{50} is the intracellular phototoxic content corresponding to the PC_{50} obtained from Fig. 2B.
[c] Data obtained from Silva et al. [5].
[d] N_3^- ions at a non-toxic concentration of 20 mM were present during the 3 h incubation with P-R and the subsequent 30 min irradiation. Data represent survival, where 100% corresponds to survival in untreated samples.

as a function of the incubation concentration for all derivatives (Fig. 2B). The relative order of magnitude of the uptake is the same as that observed in Fig. 2A.

Though incubation in FCS-supplemented culture medium is more relevant to the *in vivo* situation, incubation in serum-free HBSS has also been performed to determine whether serum proteins play any peculiar role in the uptake process. The P-R uptake profiles as a function of incubation time or of incubation concentration are found to be similar in the presence and absence of serum (data not shown). This suggests that, in contrast to the behavior of P-(Lys)$_n$, there is no strong interaction between the other P-R shown in Fig. 1 and serum proteins [6].

3.2. Photocytotoxicity of P-R derivatives

To reach maximum uptake, cells were incubated for 3 h with porphyrins in FCS-supplemented EMEM prior to irradiation. No cytotoxicity was observed with untreated sham-irradiated cells or with untreated irradiated (up to 60 min) cells in the presence of 0.5% or less DMSO in the incubation medium (data not shown). Moreover, none of these porphyrins exhibited dark cytotoxicity at incubation concentrations up to 5 μM. Fig. 2C (irradiation with increasing light doses) demonstrates that P-Me, P-DDC and P-OGal all exhibit a much larger photocytotoxicity than P-H or P-Gal at an incubation concentration of 5 μM. Conversely, lower concentrations of P-Me, P-DDC and P-OGal are sufficient to achieve high photocytotoxicity (Fig. 2D). The incubation concentrations necessary to obtain a 50% decrease in NR uptake after a 30 min irradiation can be estimated from Fig. 2D. These values, hereafter referred to as "photocytotoxic concentrations" (PC_{50}), are reported in Table 1, which also includes earlier data obtained with the P-(Lys)$_n$ derivative. Table 1 provides another photocytotoxicity index, the "intracellular phototoxic concentration" (IPC_{50}) which represents the intracellular concentration which produces a 50% decrease in NR uptake after a 30 min irradiation. Low IPC_{50} values of ~50 pmol per mg of protein are obtained with P-Me, P-DDC or P-OGal and a relative efficiency – P-OGal > P-DDC = P-Me ≫ P-Gal > P-H – is deduced from Table 1. Experiments performed after incubation in the absence of serum proteins lead to similar data for these conjugates, further illustrating that little if any role is played by serum proteins in uptake of these porphyrins (data not shown).

3.3. Oxidative stress photo-induced by P-R derivatives

Singlet oxygen is the main cytotoxin involved in PDT with porphyrins [12]. The photophysical studies here revealed no major difference in the efficiency of P-H, P-Me, P-DDC, P-OGal and P-Gal to produce singlet oxygen in a high yield whereas P-(Lys)$_n$ was found earlier to be about 4 times less effective [6,13]. Inhibition of cell photosensitization by specific $^1O_2$ quenchers such as N_3^- ions (Table 1) demonstrates the role of singlet oxygen in photo-oxidative stress induced by the tricationic porphyrins. Lipid peroxidation has been used as an overall index of oxidative stress. It has been quantified by measuring TBARS formation in cell supernatants since previous studies demonstrate practically no intracellular TBARS formation in photosensitized cells themselves. The TBARS production is shown to increase nearly linearly with the irradiation time (Fig. 3A). The ability of P-R to trigger lipid peroxidation parallels their photocytotoxic potential, and the strongly photocytotoxic P-Me, P-DDC and P-OGal as well as P-(Lys)$_n$ (see Fig. 4 in [6]), may be seen to be the most effective TBARS producers. Again, similar data were obtained in the absence of serum proteins (data not shown).

3.4. Cytotoxicity and oxidative stress photo-induced by PPIX

To compare the effects of P-R photosensitization to those of ALA, the pro-drug used in the PDT of skin lesions, cells have been incubated with various concentrations of ALA prior to irradiation in order to induce endogenous PPIX. Subsequently, the intracellular PPIX content was determined by fluorescence measurement. The photocytotoxicity or the lipid peroxidation, or both have also been determined. Data in Fig. 3B show that the IPC_{50} is approximately 50 pmol per mg of protein. About 1.8 mol of TBARS per mol of intracellular PPIX are released after a 30 min irradiation (Fig. 3C).

3.5. Fluorescence microscopy of P-R derivatives

P-R derivatives fluoresce near 660 nm and exhibit comparable fluorescence quantum yields under similar solvent conditions [13]. Fig. 4 illustrates the phase contrast and fluorescence images obtained for control cells (sham-treated cells) and for cells treated for 3 h with P-R in FCS-supplemented culture medium. The fluorescence images have been obtained with an excitation in the near UV (330–380 nm) and an emission in the red-visible range (610–700 nm). Fig. 4G–R are matching fluorescence images of the phase contrast images (Fig. 4A–F). For ready comparison, fluorescence images are displayed on the same scale in panels G–L, while they are displayed between the minimum and maximum fluorescence levels in M–R. As expected, untreated cells exhibit a very low fluorescence arising from the cytoplasm with larger intensities in the perinuclear area and the mitochondrial network. Cells treated with P-Me, P-DDC and P-OGal fluorescence more intensely, in agreement with greater uptake. A rather diffuse fluorescence with some spots in the perinuclear area is observed from cells treated with P-H and P-Gal, suggesting a main cytoplasmic and plasma membrane localization and little accumulation at specific sites. By contrast, cells treated with P-Me, P-DDC and P-OGal exhibit stronger fluorescence, mostly localized in perinuclear spots which suggests more specific localization in lysosomes or lysosome-like structures. A double labeling of the cells (Fig. 5A–C) was performed with P-R and LysoTracker Green, a lysosome specific probe emitting a green fluorescence centered towards 510 nm. As shown for P-DDC (Fig. 5B and C) the localization patterns of the green and red fluorescences are very similar, although a total superimposition cannot be achieved. This suggests a localization in other non-lysosomal structures, most probably, endocytotic or pinocytotic vesicles

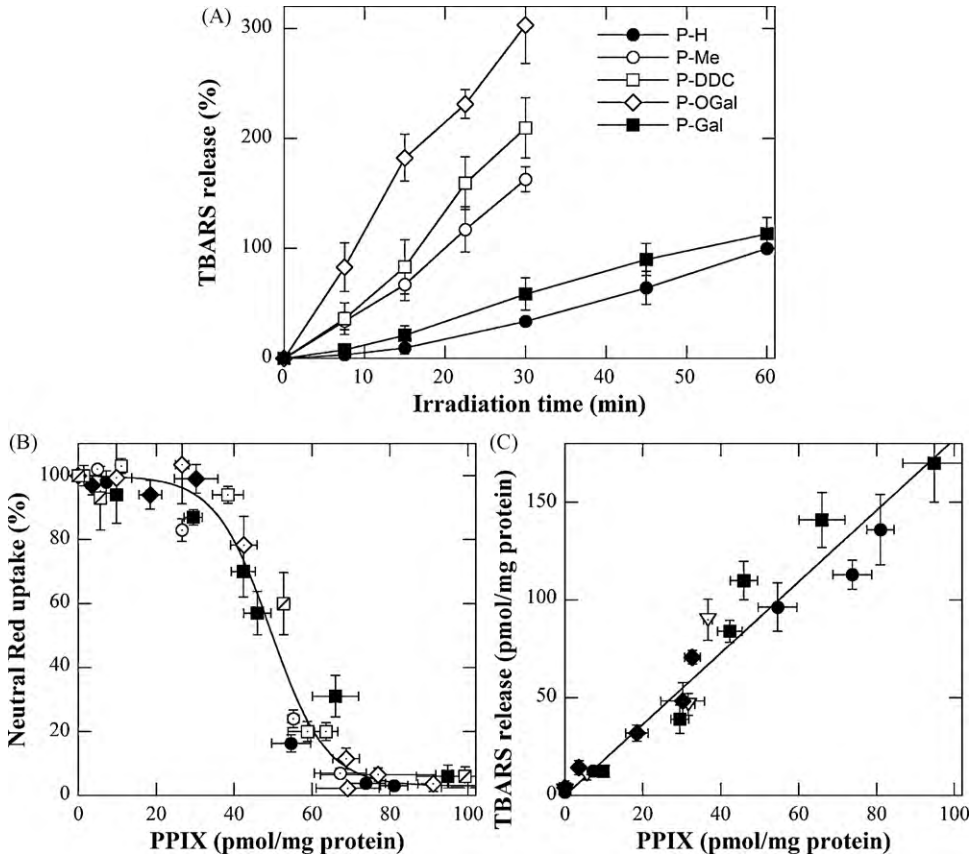

Fig. 3. (A) Lipid peroxidation photosensitized by P-H, P-Me, P-DDC, P-OGal and P-Gal (●,○,□,◇,■) after incubation for 3 h with 5 μM P-Rin FCS-supplemented culture medium prior to irradiation. TBARS released in the supernatant, normalized to the protein content, are expressed as the percentage of TBARS released after 60 min of irradiation of cells incubated with P-H (100% correspond to 37 ± 7 pmol/mg). Data are the mean of three independent experiments performed in triplicates. (B and C) Photosensitized cytotoxic effects (B) and lipid peroxidation (C) as a function of the intracellular PPIX concentration after ALA treatment. Cells were treated for 18 h without or with ALA (0.1–0.8 mM) in FCS-supplemented culture medium and irradiated for 30 min. A 100% Neutral Red uptake corresponds to sham-irradiated untreated cells. TBARS released in the supernatant were normalized to the protein content. Each symbol corresponds to an independent experiment performed in triplicates. Closed symbols in B and C correspond to data obtained from the same experiment.

beside a minor lysosomal incorporation. These vesicles have a pH higher than that of lysosomes (pH 5–6) and are therefore inefficiently labeled by LysoTracker Green®. On the other hand, lysosomal staining by the probe may be partially hidden by FRET from the probe (the donor) to P-R (the acceptor). Such behavior is observed in the case of another PDT model where tolyporphin is the photosensitizer [8]. Since P-R are positively charged, and since the inner mitochondrial membrane exhibits a negative potential, mitochondria are expected to be a preferential site for P-R localization. However, micrographs obtained with the specific mitochondrial probes, rhodamine 123 and MitoTracker® show a perinuclear network extending all over the NCTC 2544 keratinocytes (see also Gaullier et al. [14]) incompatible with the pattern of P-Me, P-DDC and P-OGal localization (Fig. 5D–F). This observation confirms previous results obtained with P-$(Lys)_n$ [6]. Although tetracationic porphyrins readily accumulate in the cell nucleus [15,16], the fluorescence depression on the nuclear area observed for all P-R strongly suggests very little, if any, localization in the nucleus of NCTC 2544 keratinocytes.

3.6. Mechanisms of the PDT-induced death in NCTC 2544 cells

Necrosis induced *in vitro* by PDT with porphyrins has long been established, and is essentially characterized by increased cell volume, organelle swelling and plasma membrane alterations [17]. Apoptosis and autophagy are induced by a variety of stress factors, notably those encountered in cancer therapies. Two reviews have been recently published on guidelines concerning the use and interpretation of assays for determining mechanisms of cell death [18,19]. It is of interest to understand the death mechanisms underlying the efficient photocytotoxicity of P-Me, P-OGal and P-DDC. As P-Me, P-OGal and P-DDC exhibit similar intracellular localization, P-OGal – the most effective photosensitizer – was chosen as representative P-R for this study.

3.7. Is apoptosis involved in P-R photocytotoxicity?

Translocation of phosphatidylserine from the inner layer to the outer layer of the plasma membrane is observed in the initial stages of apoptosis. To detect this translocation, we used annexin V, a protein that binds to cells with exposed phosphatidylserine. A simultaneous cytometric analysis of annexin V binding and propidium iodide uptake by dead cells was carried out. According to Fig. 3A, incubation with 5 μM P-OGal for 3 h, followed by a 15 min irradiation, leads to about 25% cell killing. However, no significant change in the percentage of annexin V positive cells (Fig. 6A) could be observed up to 9 h following irradiation. Similar results were observed after a 3 h incubation of cells with 1 μM P-OGal followed by 15 min of irradiation or with 5 μM P-OGal followed by 30 min of irradiation (data not shown).

Another hallmark of apoptosis is nuclear DNA breakdown into oligonucleosomal units of about 200 bp. The enzyme-linked immunosorbent assay used to quantify the cytoplasmic accumulation of histone-associated DNA fragments shows no significant increase in cytoplasmic histone-associated DNA fragments 0, 1, 3, 6, 9 12 h (Fig. 6B) or 24 h (data not shown) after PDT with 5 μM P-OGal.

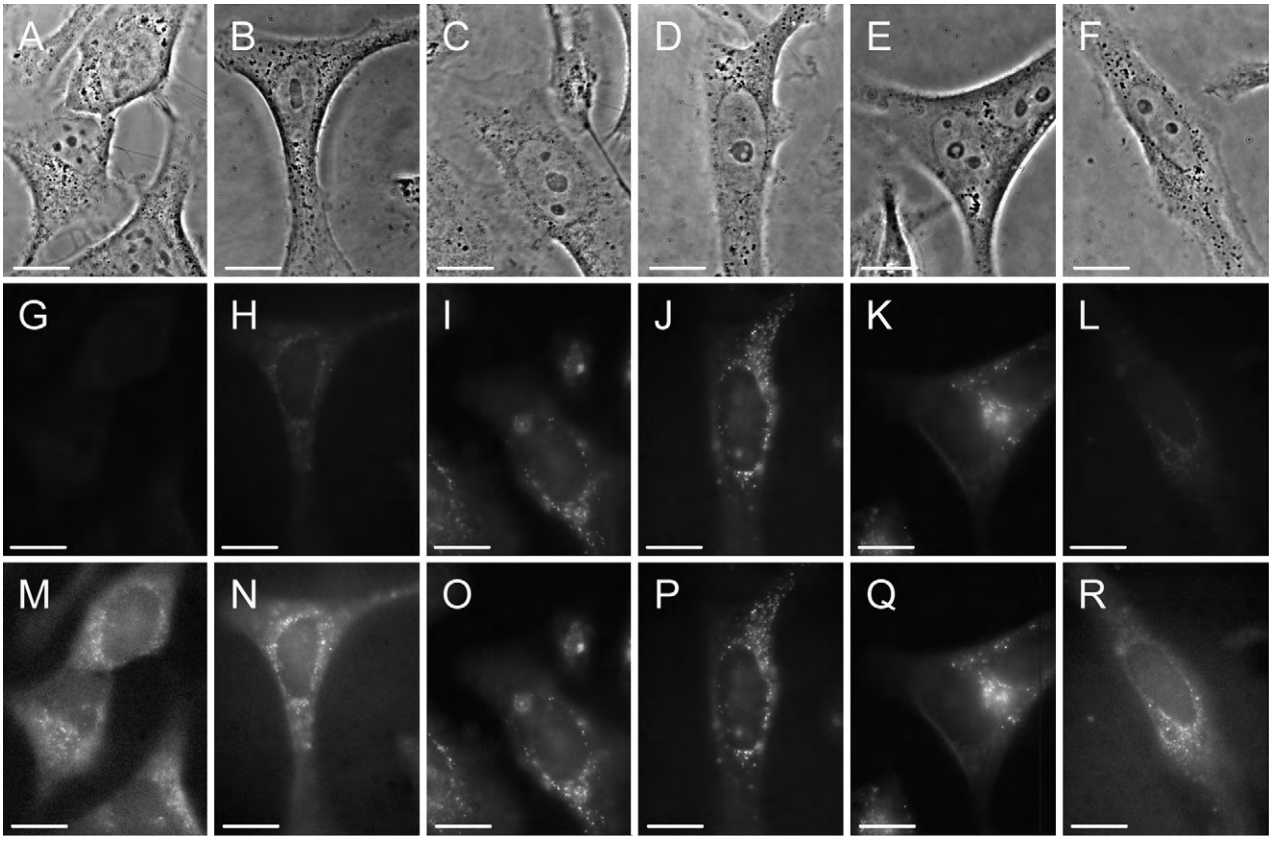

Fig. 4. (A–R) Phase contrast images (A–F) and fluorescence micrographs (G–R) obtained with NCTC 2544 keratinocytes incubated for 3 h in EMEM + 10% FCS with no additives (A, G, M), with 5 μM P-H (B, H, N), P-Me (C, I, O), P-DDC (D, J, P), P-OGal (E, K, Q) or P-Gal (F, L, R). Fluorescence images were obtained with a Nikon ×100 oil immersion objective. Exposure time: 2 s. Signal attenuation: 1/16. Dichroic mirror: 400 nm. Excitation: 330–380 nm. Emission: 610–700 nm. G–L: 256 grey levels between 0 and the maximal fluorescence recorded with P-DDC (show relative intensities). M–R: 256 grey levels between 0 and individual fluorescence (show the topography of localization). White bar = 20 μm.

Activation of intracellular proteases called caspases, is a key event during apoptosis. The caspase cascade is regulated through their partial cleavage. To further examine whether apoptosis is involved in the P-R-induced photokilling, caspase-3, caspase-8 and caspase-9 activities have been assayed. Cleavage of proteins by caspases leads to chromatin condensation and DNA degradation. Several families of PDT photosensitizers (porphyrins, chlorins, phthalocyanines.) are strong inducers of apoptosis in various cell lines [12]. Because apoptosis is a dynamic process, samples have been collected up to 24 h following PDT. No evidence for cleavage of the caspase-3, caspase-8 and caspase-9 substrates was found after P-OGal-PDT under the conditions outlined above (see Fig. S1 in supplementary data). The absence of procaspase-3, procaspase-8 and procaspase-9 cleavage in Western blots, also shown in the supplementary data, confirms the lack of caspase activities. In addition, no cytochrome *c* leakage has been observed with P-OGal photosensitized cells (Fig. 7A). To verify that under our experimental conditions, NCTC 2544 cells may readily undergo apoptosis, such cells were incubated 30 min with 10 μM 5-methoxypsoralen in DPBS and then were subjected to UVA irradiation (2.5 J/cm^2). Twenty four hours later, NCTC 2544 treatment with 5-methoxypsoralen + UVA had resulted in extensive activation of caspase-3 (6-fold increase in activity) and caspase-9 (2-fold increase in activity) in cell lysates. No change in activity was observed with caspase-8 (data not shown). These results are fully consistent with those previously presented by Viola et al. [20]. Another positive control was performed by treating cells with 5 μM campothecin. Measurement of caspase-3 activity and flow cytometry after PI and Annexin V staining readily show apoptosis induction only 9 h after treatment. These data support the conclusion that apoptosis induction after photodynamic injury induced by P-R is insignificant.

3.8. Autophagy of NCTC 2544 keratinocytes after PDT with tricationic porphyrins

Autophagy is a normal process that helps the cell get rid of damaged organelles or macromolecules. This highly regulated process is morphologically evidenced by the formation of autophagosomes and autolysosomes [18,21]. Recently, a new form of programmed cell death characterized by autophagic hallmarks has been discussed [18,19]. To determine if programmed cell death associated with PDT might exhibit such characteristics, we monitored the autophagic activity in NCTC cells exposed to P-OGal. Autophagic activity was followed using a fluorescent marker (GFP-LC3) consisting in a fusion microtubule-associated protein light-chain 3 (LC3) tagged with a green fluorescent protein (GFP). Upon autophagy induction, LC3 is proteolytically processed and recruited to autophagosomal membranes [11]. After P-OGal PDT, we have observed the subcellular redistribution of the fluorescent marker GFP-LC3 fusion protein from a uniform, cytosolic, to a punctated, vacuolar pattern [18,19] (Fig. 7A). After a 3 h incubation of cells with 5 μM P-OGal, followed by 15 min of irradiation, a time-dependent increase in the number of cells showing the characteristic vacuolar pattern of GFP-LC3 is observed (Fig. 7B). By contrast, no significant change in the accumulation of GFP-LC3 is observed (Fig. 7B) after incubation of NCTC 2544 cells with 0.8 mM ALA for 18 h followed by a 15 min irradiation, which induces similar photocytotoxic effects as those observed with P-R (see Fig. 3C).

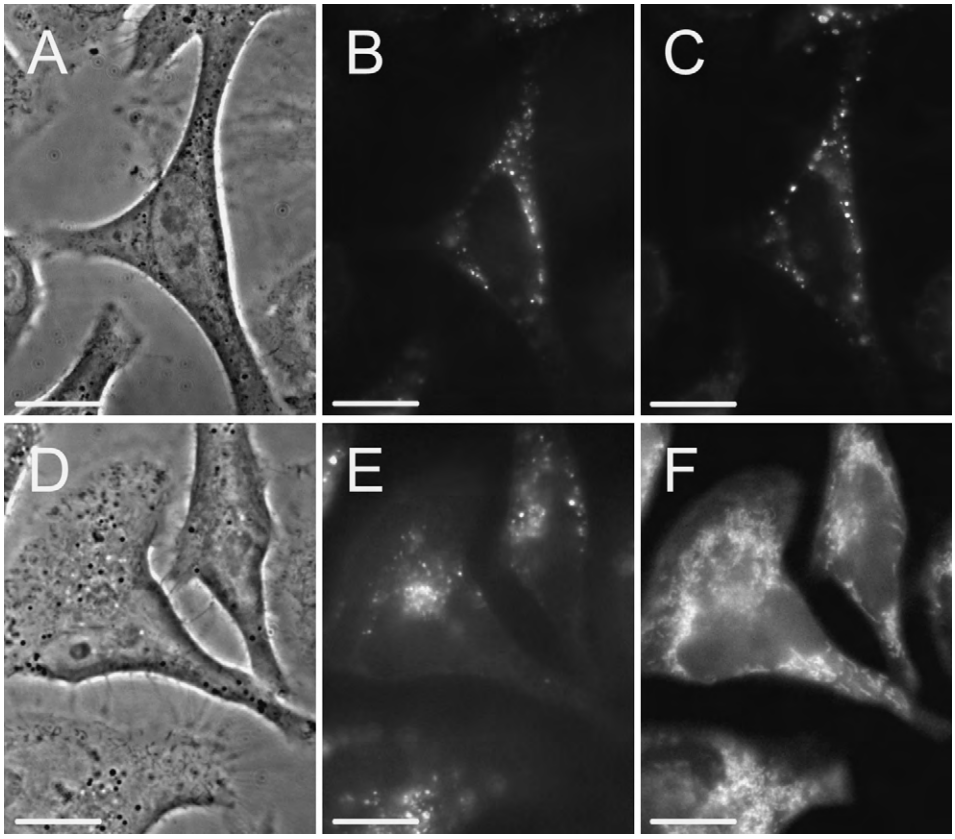

Fig. 5. Double-labeling experiments: (A–C) Phase contrast images (A) and fluorescence micrographs (B and C) obtained after incubation for 3 h with 5 μM P-DDC in EMEM + 10% FCS and then for 30 min with 5 μM P-DDC and 125 nM LysoTracker Green in EMEM + 10% FCS. (D–F) Phase contrast images (D) and fluorescence micrographs (E and F) obtained after incubation for 3 h with 5 μM P-DDC in EMEM + 10% FCS and then for 30 min with 5 μM P-DDC and 10 μM Rhodamine 123 in EMEM + 10% FCS. Objective, signal attenuation, dichroic mirror and excitation as in Fig. 4. Exposure times: 2 s with the red emission filter and then 2 s with the green emission filter. Emission: 610–700 nm (B and E) and 510–565 nm (C and F). White bar = 20 μm.

In another series of measurements, the immunoblotting analysis for the modulation of the p62 protein, also called sequestosome 1 (SQSTM1), by P-R has been performed. Since p62/SQSTM1 accumulates when autophagy is inhibited and decreases when autophagy is induced, it may be used as a marker of autophagic activity [18]. Western blotting analysis reveals that 6 h after irradiation the amount of p62/SQSTM1 is decreased by more than 60% in the P-OGal-treated cells but not in cells treated with P-OGal but not irradiated (Fig. 7D).

To further assess a possible contribution of autophagy to P-OGal-induced cell death, we have studied the effect of 3-methyladenine (3-MA), a well-characterized autophagy inhibitor [18]. After 15 min of irradiation of cells incubated for 3 h with 5 μM P-OGal and 5 mM 3-MA, the percentage of cells showing the characteristic vacuolar pattern of GFP-LC3 in the P-OGal + 3-MA-treated group is decreased to about 70% of the value obtained with the group treated with P-OGal alone (Fig. 7C). By contrast P-OGal-induced cell death is inhibited by about 40% after incubation with 5 mM 3-MA (Fig. 6C). It is well established that the inhibition of autophagy by 3-MA may potentiate apoptosis induced by a variety of chemicals [21]. Autophagy inhibition does not significantly change the percentage of annexin V positive cells measured 6 h after P-OGal-PDT (Fig. 6C). Furthermore, no leakage of mitochondrial cytochrome *c* in the cytoplasm has been observed with 3-MA-treated cells up to 6 h after irradiation (data not shown), but the p62 degradation was decreased by about 80% (Fig. 8D).

These data suggest that cells undergoing P-OGal-PDT show increased autophagy levels and that autophagy may be associated with cell death induced by P-OGal photosensitization.

3.9. MAPK participate in death of NCTC 2544 keratinocytes after PDT with tricationic porphyins

Several lines of evidence indicate that MAPK participate in closely related signaling cascades that contribute to the regulation of gene expression in response to photodynamic treatment. Activation of ERK 1/2 is generally associated with cell proliferation and survival, while p38 and JNK are linked to induction of apoptosis [12,22]. Recent reports show, however, that the role of MAPKs in cell death induced by photosensitization is largely cell type and photosensitizer-dependent [12].

The MAPK phosphorylation has been assessed in NCTC 2544 cells treated by P-OGal-PDT and lysed 0, 1, 3, 6 or 9 h after irradiation. The p38 and JNK phosphorylation was significantly increased. This increase is stronger with p38 and maximal 3 h after irradiation (Fig. 8A). After this interval, p38 and JNK phosphorylation steadily declines, becoming barely detectable 9 h after irradiation. On the other hand, no significant phosphorylation of p38 and JNK is observed before irradiation in untreated (control) cells or after sham-irradiation of P-OGal-treated cells.

Regarding Akt and ERK, the level of total Akt and ERK is unchanged whereas the p-Akt and p-ERK levels are markedly decreased after P-OGal-PDT in a time dependent manner (Fig. 8A). In contrast to results obtained with p38 and JNK, substantial amounts of phosphorylated ERK1/2 and Akt are detected prior to irradiation. Although the p-ERK and p-Akt levels remain unchanged in sham-irradiated cells and untreated controls, p-Akt decreased progressively after the photodynamic challenge while p-ERK has a significant abrupt drop at 3 h and becomes barely detectable. These results suggest that MAPKs

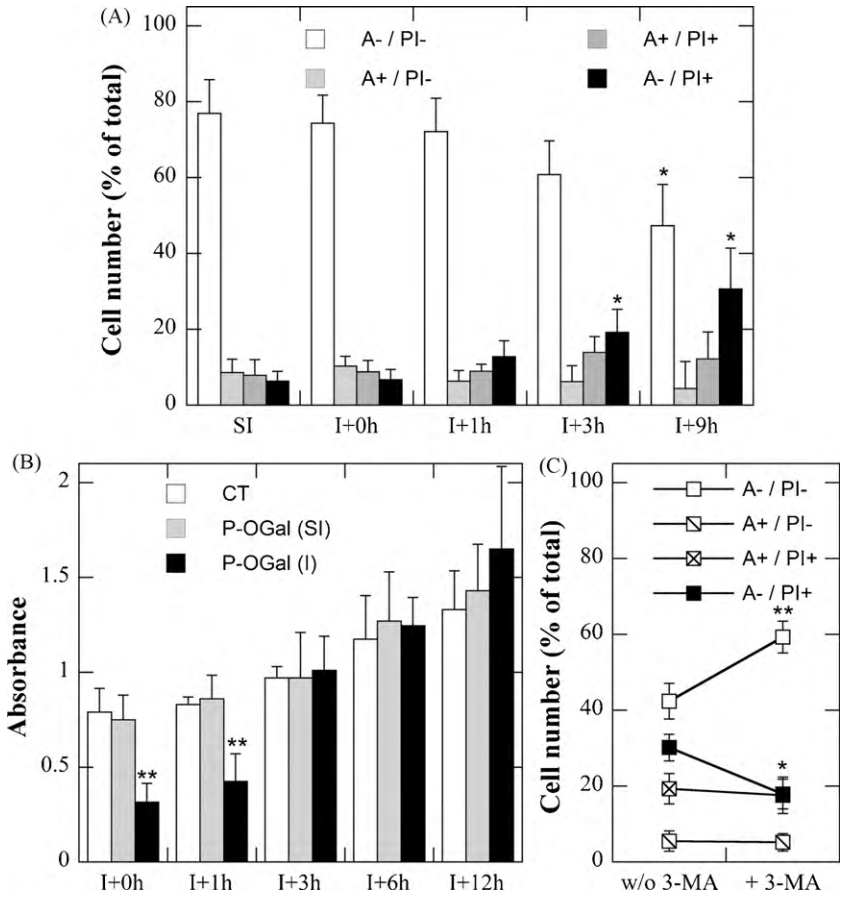

Fig. 6. (A) Flow cytometric analysis of NCTC 2544 keratinocytes after P-OGal photosensitization. Cells were incubated for 3 h with 5 μM P-OGal in FCS-supplemented culture medium, then irradiated (I) or sham-irradiated for 15 min (SI). They were stained with Annexin V-FITC and PI and analyzed by flow cytometry at the indicated times after irradiation (I+). Data are the mean of 3 independent experiments performed in triplicates. A−/PI−: viable cells; A+/PI−: still viable cells undergoing apoptosis (early apoptotic cells); A+/PI+: late apoptotic dead cells; A−/PI+: necrotic cells. $^{*}p < 0.05$ compared to matching SI. SI data were obtained immediately after sham-irradiation and were unchanged for durations up to 9 h after sham-irradiation. (B) After incubation and irradiation as in (A), cell lysates were prepared and analyzed for cytoplasmic accumulation of histone-associated DNA fragments by an enzyme-linked immunosorbent assay at the indicated times after irradiation. CT: sham-treated control cells; P-OGal (SI): treated cells but sham-irradiated for 15 min; P-OGal (I) cells treated and irradiated for 15 min. Data are the mean of 3 independent experiments performed in triplicates. $^{**}p < 0.01$ compared to matching CT. (C) Effect of 3-MA on cytotoxic effects photosensitized by P-OGal. Before irradiation, cells were treated for 3 h with 5 μM P-OGal only (w/o 3-MA) or simultaneously with 5 μM P-OGal and 5 mM 3-MA. Cells were stained with Annexin V-FITC and PI 6 h after irradiation and analyzed by flow cytometry. Data are the mean of 3 independent experiments performed in triplicates. $^{*}p < 0.05$ and $^{**}p < 0.01$ compared to 3-MA untreated cells.

activity modulation by P-OGal-PDT may be implicated in the cytotoxicity.

To examine the role of MAPKs activation in cell death, P-OGal-treated cells were pre-incubated with the p38 (SB203580) and JNK (SP600125) inhibitors. As a matter of fact, SB203580 and SP600125 inhibit p38 and JNK phosphorylation in the NCTC 2544 cells. Thus, after an osmotic stress induced by 0.4 M sorbitol for 10 min, immunoblot analysis demonstrates that 25 μM SB203580 and 25 μM SP600125 reduced p-p38 and p-JNK over 75% of the control value (data not shown). Addition of SP600125 3 h before irradiation, increases the photo-induced cell death by approximately 50%, whereas SB203580 has no significant effect (Fig. 8B). Incidentally, it must be noted that the viability of control cells treated with P-OGal and pre-incubated with SB203580 and SP600125 but left in the dark was unchanged. Fig. 8B also suggests that an insignificant effect on the percentage of annexin V positive cells is observed 6 h after P-OGal-PDT of cells pre-incubated with 25 μM of p38 and JNK inhibitors. By contrast, 6 h after irradiation, the number of cells showing the vacuolar pattern of GFP-LC3 is increased by 31% ($p < 0.001$) in cells treated with P-OGal and 25 μM SP600125 (Fig. 8C) although SP600125 has no effect on the basal level of GFP-LC3-puncta. On the contrary, no significant change has been observed in the P-OGal PDT-induced accumulation of GFP-LC3 after pre-incubation of cells with SB203580. Under the same experimental conditions, SP600125 but not SB203580 increases the p62 degradation after PDT (Fig. 8D). Taken together, these results suggest that JNK exerts a negative regulator effect on P-OGal PDT-induced autophagy and PDT-dependent programmed cell death.

4. Discussion

4.1. The nature of the conjugated chain determines the intracellular localization of tri-cationic conjugates and their cytotoxicity

The comparison of the photocytotoxic potential of P-R is straightforward since they absorb identical light under the same experimental conditions (see supplementary data). The greater photocytotoxic efficiency of P-OGal, P-DDC and P-Me compared to that of P-H and P-Gal (Fig. 2C,D) parallels the magnitude of the lipid peroxidation (Fig. 3A) suggesting that their phototoxicity and their overall ability to produce an oxidative stress correlate, irrespective of the targets in the cell lines studied.

Interestingly, P-OGal, P-DDC and P-Me favorably compare with endogenous PPIX produced by ALA treatment. Fig. 3B demonstrates that a 50% loss in Neutral Red uptake is obtained with an intracellular PPIX concentration (~50 pmol/mg of cellular protein) similar to that found for P-OGal, P-DDC and P-Me. Since light doses absorbed by equal concentrations of P-R and PPIX are essentially

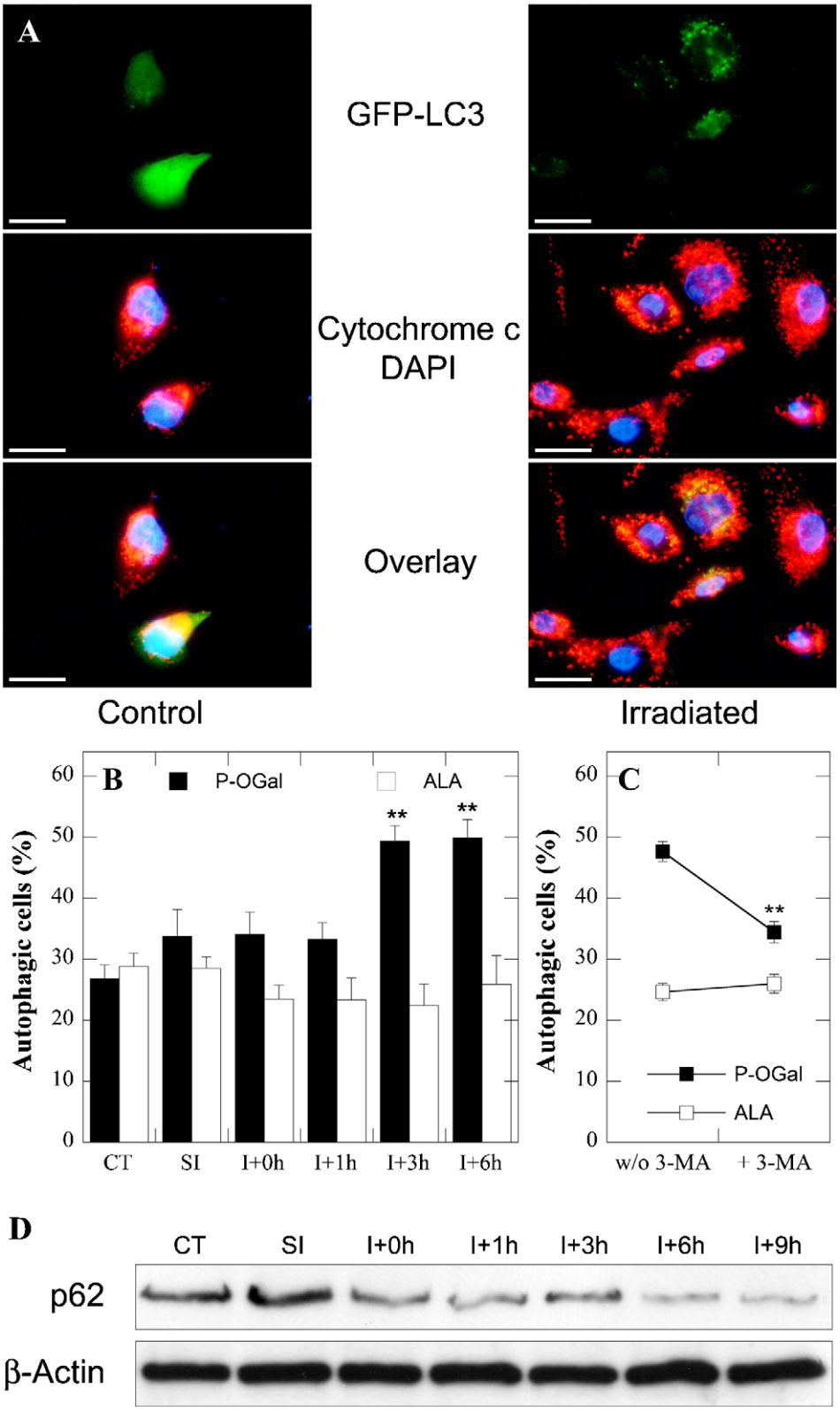

Fig. 7. P-OGal induced autophagic cell death in NCTC 2544 keratinocytes. (A) Cells transfected with GFP-LC3 (green) were treated for 3 h with 5 μM P-OGal and then irradiated for 15 min. Fluorescence micrographs were simultaneously recorded after cytochrome *c* immunofluorescent staining (red) and nucleus staining with 4,6-diamidino-2-phenylindole (DAPI; blue). Images are representative of cells with 3 or more puncta of GFP-LC3. Whereas untreated healthy cells (Control) show diffuse distribution of GFP-LC3, 6 h after irradiation, P-OGal treatment (Irradiated) induces GFP-LC3 puncta indicating the formation of autophagosomes. Transfected cells treated with 0.8 mM ALA for 18 h and irradiated for 15 min give essentially the same puncta distribution as untreated cells (not shown). Simultaneously, unirradiated healthy cells display a cytochrome *c* perinuclear rod-like pattern consistent with location in mitochondria. A puntacte pattern with no diffuse cytoplasmic distribution of fluorescence is observed in irradiated cells suggesting that cytochrome *c* remains in mitochondria. White bar = 20 μm. (B) Transfected cells treated with P-OGal or ALA presenting 3 or more GFP-LC3 vesicles were counted at indicated times after irradiation (I+). CT: controls (sham-treated sham-irradiated cells); SI: cells treated with P-OGal or ALA but sham-irradiated. Results from 3 independent experiments in triplicates are given as a percentage of autophagic cells over 500 transfected cells (mean ± SD). $^{**}p < 0.01$ compared to matching CT. SI data were obtained immediately after irradiation and were unchanged up to 6 h after sham-irradiation. Sham-treated irradiated cells behave as CT. (C) Cells

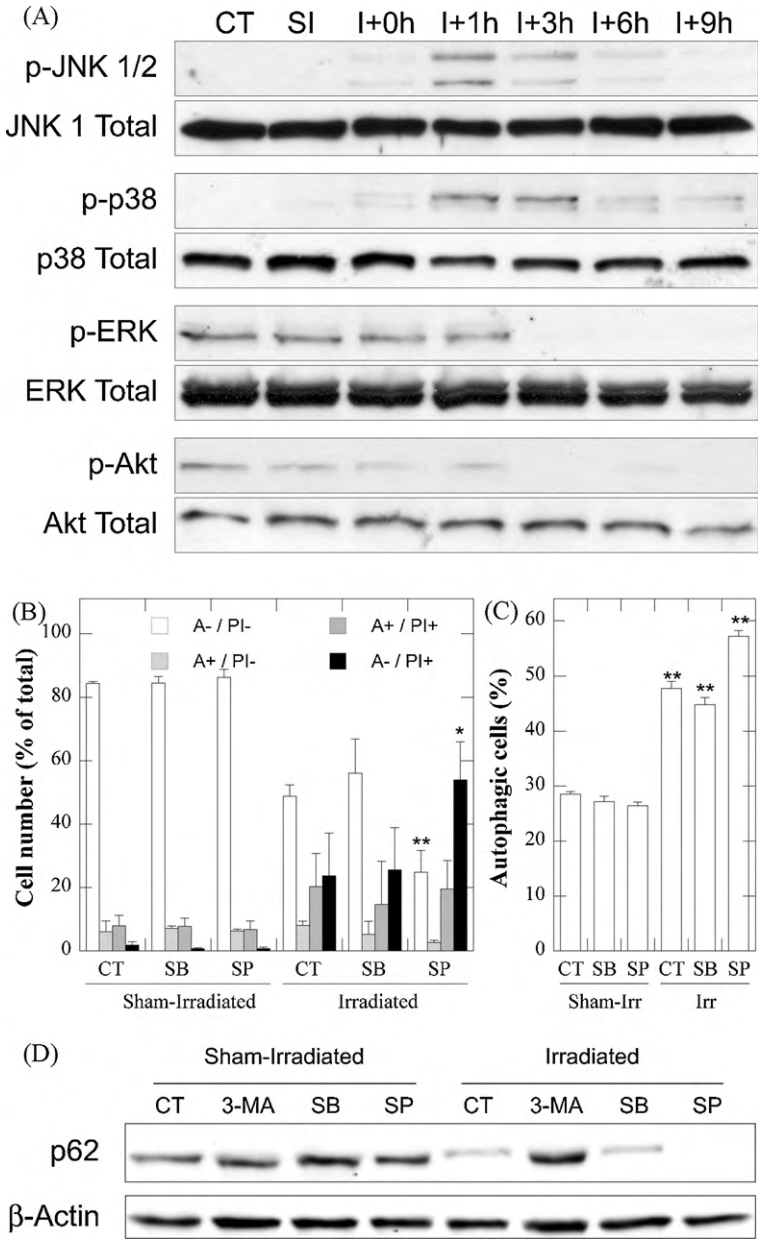

Fig. 8. MAPKs protein expressions were analyzed in lysates of NCTC 2544 cells. (A) Representative Western blots of total and phosphorylated JNK, p38, ERK and Akt either in cells untreated but left in supplemented culture medium for 3 h (control, CT) or in cells treated during 3 h with 5 μM P-OGal and then sham-irradiated (SI) or irradiated for 15 min and incubated for indicated times after irradiation (I+). Total-JNK, p38, ERK and Akt immunoblottings are used as controls for protein loading. (B) Effect of 25 μM SB203580 or 25 μM SP600125 on cytotoxic effects photosensitized by P-OGal. Before irradiation, cells were treated for 3 h with 5 μM P-OGal (CT) or with 5 μM P-OGal and 25 μM SB203580 (SB) or SP600125 (SP). Nine hours after irradiation, cells were stained with annexin V-FITC and PI and analyzed by flow cytometry. Data are the mean of 3 independent experiments performed in triplicates. $^{*}p < 0.05$ and $^{**}p < 0.01$ compared to irradiated CT. (C) Cells transfected with GFP-LC3 were treated using P-OGal without (CT) or by pre-incubation with 25 μM SB203580 (SB) or SP600125 (SP). Autophagic cells were counted and results are given as in Fig. 7B (mean ± SD of 3 independent experiments in triplicates). $^{**}p < 0.01$ compared to matching sham-irradiated cells. (D) Western blotting analysis of p62 in lysates from cells collected 9 h after P-OGal-PDT without or with pre-incubation in the presence of 5 mM 3-MA (3-MA), 25 μM SB203580 (SB) or SP600125 (SP). β-actin is shown as loading control.

identical (see supplementary data), P-OGal, P-DDC and P-Me are photosensitizers as powerful as PPIX in our cell model. Comparison of data in Figs. 2B and 3A and C demonstrates that at equivalent light doses, oxidative membrane damage is more pronounced with PPIX than with P-Me, P-DDC or P-OGal. This behavior is consistent with the higher hydrophobicity of PPIX favouring its intracellular localization in lipophilic microenvironments.

With the exception of P-$(Lys)_n$, P-R derivatives have comparable singlet oxygen formation quantum yield. Consequently, they have similar intrinsic photosensitizing potential. From Fig. 2B, it may be estimated that incubation with P-Me, P-DDC or P-OGal concentrations in the range 0.7–0.8 μM leads to the same P-R intracellular contents as incubations with 5 μM P-H or 1.4–1.6 μM P-Gal. It may be deduced from Fig. 2C and D that these differences cannot account for the observed differences in cytotoxicity.

The intracellular localization may explain different photocytotoxic responses. Microfluorometry confirms that P-H and P-Gal are taken up less by NCTC 2544 keratinocytes than is P-Me, P-DDC or

transfected with GFP-LC3 were treated with P-OGal or ALA and irradiated as described in (A), without or with simultaneous treatment with 5 mM 3-MA. Autophagic cells were counted and results are given as in B (mean ± SD of 3 independent experiments in triplicates). $^{**}p < 0.01$ compared to matching 3-MA-untreated cells. (D) Western blotting analysis of lysates from cells collected at indicated times after treatment with P-OGal and irradiation. Total cell lysates were analyzed for p62. β-actin is shown as loading control. SI data were obtained immediately after sham-irradiation and were unchanged up to 9 h after sham-irradiation. Sham-treated irradiated cells behave as CT.

P-OGal, whose fluorescence is more specifically localized in spots that may correspond to endo- or pinocytotic vesicles, but not to mitochondria and nucleus. The observations reported here demonstrate that the nature of the conjugated side chain is more critical than the electric charge of the porphyrin ring in controlling the uptake and site of localization of the P-R and, consequently, their greater photosensitizing efficiency. It may be thought that major direct damage to the mitochondria and the nucleus by $^1O_2$ produced by P-R is rather unlikely since $^1O_2$ does not diffuse a great distance from its site of production [16].

4.2. The photo-induced cell death shows hallmarks of autophagy

Beside demonstrating for the first time the chain structure dependence of the photocytotoxic potential of tri-cationic porphyrins, this study provides new information about mechanisms of cell death and MAPK-mediated stress signaling in our PDT model. It has been demonstrated that many PDT photosensitizers including those used to treat skin lesions in clinical practice, e.g. ALA and photofrin®, activate several pathways leading to apoptosis ([12] and references therein). Our results are in sharp contrast with these reports. Consistent with the absence of apoptosis, no annexin V cell staining (Fig. 6A), no oligonucleosome fragmentation (Fig. 6B) and no caspase activation (see supplementary data) are observed after P-OGal-PDT. Among other factors, these results may be related to the non-mitochondrial localization of the most photocytotoxic P-R (Fig. 4). The absence of major mitochondrial damage is also suggested by the lack of cytochrome *c* leakage (Fig. 7A). On the other hand, we show the appearance of a punctate pattern of GFP-LC3 and a decrease in the amount of p62 following PDT with P-OGal (Fig. 7A–C). Consistently, 3-methyladenine, a well-known inhibitor of autophagy, inhibits the photocytotoxicity, lowers the percentage of cells showing punctate GFP-LC3 and decreases p62 degradation (Figs. 6C, 7C and 8D). The incorporation of P-R in lysosomes or pre-lysosomes in the vicinity of the ER and the Golgi apparatus might be responsible for this conjunction of pro-autophagic and anti-apoptotic events.

There are relatively few recent reports on the induction of autophagy by photodynamic therapy and most deal with apoptosis-deficient cells or cells whose caspase activity has been inhibited [12,23]. We used apoptosis-competent cells in which porphyrin conjugates induced autophagic cell death in the absence of apoptosis inhibitor. Treatment with the autophagy inhibitor 3-MA is not associated with a significant change in the percentage of annexin V positive cells and thus with apoptosis activation (Fig. 6C). Possibly, autophagy may constitute an attempt by cells to remove photo-oxidized organelles or large cross-linked aggregates formed after photodynamic damage to protein complexes.

4.3. Consequences of P-OGal-PDT on MAPKs in NCTC 2544 cells

Several studies performed with different cell lines and photosensitizers have shown that MAPKs participate in the oxidative signaling events induced by PDT [12]. Previous research presented conflicting data concerning the roles of p38 and JNK in cell viability after PDT. Results suggest that the degree of p38 and JNK phosphorylation as well as their effect on cell death regulation after PDT may depend on cell type, photosensitizer and light dose [22,24]. In contrast to apoptosis, relatively little is known about PDT-induced autophagy signaling in terms of MAPK activation and possible cross-talk among different pathways.

The role of JNK in cell death has long been controversial as it exhibits a pro-survival function or it promotes lethality depending on the physiological or pathological condition studied [25]. The paradoxical nature of this effect could be partially due to different modes of JNK activation [26], different kinetics [27] or might depend on the nature of the chemical inducers used including reactive oxygen species [26,28]. An early transient JNK activation determines cell survival whereas sustained JNK activation can induce cell death signals [27]. Consistent with these data, we observed a rapid and transient JNK activation after P-OGal-PDT associated with a negative regulatory effect on cell mortality and autophagy (Fig. 8A). We may speculate that this effect might be partially explained by JNK1 mediated Bcl-2 phosphorylation known to inhibit the binding of Bcl-2 to Beclin 1 which activates autophagy [29]. Of note, it has recently been reported that JNK activation, induced by 2-methoxyestradiol in Ewing sarcoma cells, modulates autophagy either through Bcl2 phosphorylation or up regulation of the damaged regulated autophagy modulator [30,31].

While several reports support the role of p38 as inhibitor of autophagy [32], others imply the opposite [33]. Although we observed a p38 activation after P-OGal PDT, our data suggest that p38 is not directly implicated in induction of cell death. A downstream event in the mitogenic pathway is ERK activation through binding of ligands to extracellular growth factor receptors involved in regulation of growth and cell cycle progression. The Ras/Raf/ERK activation pathway can promote opposite pro-survival or anti-proliferative cellular responses, such as apoptosis and autophagy. This wide variety of processes triggered by the activation of a single pathway depends on the timing, duration and strength of activation, on subcellular localization and on the presence of reactive oxygen species (ROS) [34]. Available evidence suggests that the photooxidative stress induced by PDT may modulate ERK activity as does other ROS such as H_2O_2, which is produced in a variety of tumor cell lines by 1,3-dibutyl-2-thiooxo-imidazolidine-4,5-dione [35]. Depending on the photosensitizer and cell culture, ERK phosphorylation variably responds to the PDT-induced oxidative stress by irreversible inhibition [24], moderate attenuation [36], insignificant modulation [22] or transient activation [37]. It is noteworthy that ALA-PDT has no effect on ERK expression in HaCat cells [38]. We found a decrease in the p-ERK content to almost undetectable levels 3 h after P-OGal-PDT despite high pre-existing expression (Fig. 8A).

Activation of PI3-K/Akt is another important signaling pathway. The Akt acts on a variety of ways including mTOR activation, Bad phosphorylation, IκB kinase phosphorylation and caspase-9 inhibition, thereby preventing cell death [21]. The PDT effect on Akt regulation varies from de-phosphorylation and subsequent activation of caspase-assisted death [39] to phosphorylation stimulation [40]. Our results show a time-dependent decrease in the content of p-Akt after PDT treatment (Fig. 8A), consistent with increased photo-induced autophagic death.

5. Conclusions

Beside necrosis, autophagy may contribute to the death of NCTC 2544 keratinocytes by P-OGal-PDT with no evidence for significant apoptosis. JNK activation exerts a negative regulatory effect on photocytotoxicity and autophagy while p38 activation is not involved in cell death. Several studies show that ERK and PI3-K/Akt pathways are aberrant in human cancers [41] suggesting them as targets for the development of novel cancer treatments [42]. The inhibition of ERK1/2 and Akt activities suggests that water-soluble tri-cationic porphyrins may thus play a beneficial role in cancer treatment by PDT given their potentially easy formulation. However, the role of MAPKs modulation on photocytotoxicity and autophagic cell death induced by P-OGal-PDT still needs clarification. In this regard, the use of the siRNA technology would of definite interest to understand the role played by the JUNK pathway in the photo-induced death mechanism. Finally, the present study has allowed the characterization of P-OGal as the

most potent photoactive conjugate in the NCTC 2544 cell model. In view of its potential interest as a PDT photosensitizer in dermatology, it would also be valuable to assess its photobiological activity towards SCC or BCC cell lines.

Acknowledgements

This work was supported by an INSERM/GRICES exchange agreement, a Franco-Portuguese "PESSOA" exchange program (07958NF), a co-tutelage "PAUILF" Franco-Portuguese program (J.N.S., P.F., J-C.M., R.S., P.M.) and grants from the Gulbenkian Foundation (J.N.S., P.F.) and the "Fundação para a Ciência e a Tecnologia" (J.P.C.T., M.G.P.M.S.N., E.M.P.S., J.A.S.C.). A portion of the epifluorescence microscopy experiments was performed with the equipment of the "Centre de Microscopie du Muséum". The authors wish to thank Drs. M. Gèze and M. Dellinger for their advices. The authors wish to thank Pr. L.K. Patterson (Radiation Laboratory, University of Notre Dame, Notre Dame, Indiana) for his careful reading of the manuscript and improvement of the English language. We thank Drs. Yoshimori and Mizshima (Tokyo Metropolitan Institute of Medical Science, Japan) for the kind gift of the GFP-LC3 construct.

Appendix A. Supplementary data

Supplementary data associated with this article can be found, in the online version, at doi:10.1016/j.bcp.2010.07.033.

References

[1] Soler AM, Warloe T, Berner A, Giercksky KE. A follow-up study of recurrence and cosmesis in completely responding superficial and nodular basal cell carcinomas treated with methyl 5-aminolaevulinate-based photodynamic therapy alone and with prior curettage. Br J Dermatol 2001;145:467–71.
[2] Conneely A, Smyth WF, McMullan G. Study of the white-rot fungal degradation of selected phthalocyanine dyes by capillary electrophoresis and liquid chromatography. Anal Chim Acta 2002;2002:259–70.
[3] Zhao B, Yin JJ, Bilski PJ, Chignell CF, Roberts JE, He YY. Enhanced photodynamic efficacy towards melanoma cells by encapsulation of Pc4 in silica nanoparticles. Toxicol Appl Pharmacol 2009;241:163–72.
[4] Chen X, Hui L, Foster DA, Drain CM. Efficient synthesis and photodynamic activity of porphyrin-saccharide conjugates: targeting and incapacitating cancer cells. Biochemistry 2004;43:10918–29.
[5] Tomé JPC, Neves MGPMS, Tomé AC, Cavaleiro JAS, Soncin M, Magaraggia M, et al. Synthesis and anti-bacterial activity of new poly-S-lysine-porphyrin conjugates. J Med Chem 2004;47:6649–52.
[6] Silva JN, Haigle J, Tomé JP, Neves MG, Tomé AC, Mazière J-C, et al. Enhancement of the photodynamic activity of tri-cationic porphyrins towards proliferating keratinocytes by conjugation to poly-S-lysine. Photochem Photobiol Sci 2006;5:126–33.
[7] Tomé JPC, Silva EMP, Pereira AMVM, Alonso CMA, Faustino MAF, Neves MGPMS. et al. Synthesis of neutral and cationic tripyridylporphyrin-D-galactose. Bioorg Med Chem 2007;15:4705–13.
[8] Morlière P, Mazière J-C, Santus R, Smith CD, Prinsep MR, Stobbe CC, et al. Tolyporphin: a natural product from cyanobacteria with potent photosensitizing activity against tumor cells in vitro and in vivo. Cancer Res 1998;58:3571–8.
[9] Reyftmann J-P, Morlière P, Golstein S, Santus R, Dubertret L, Lagrange D. Interaction of human serum low density lipoproteins with porphyrins: a spectroscopic and photochemical study. Photochem Photobiol 1984;40:721–9.
[10] Filipe P, Silva JN, Haigle J, Freitas JP, Fernandes A, Santus R, et al. Contrasting action of flavonoids on phototoxic effects induced in human skin fibroblasts by UVA alone or UVA plus cyamemazine, a phototoxic neuroleptic. Photochem Photobiol Sci 2005;4:420–8.
[11] Kabeya Y, Mizushima N, Ueno T, Yamamoto A, Kirisako T, Noda T, et al. LC3, a mammalian homologue of yeast Apg8p, is localized in autophagosome membranes after processing. EMBO J 2000;19:5720–8.
[12] Buytaert E, Dewaele M, Agostinis P. Molecular effectors of multiple cell death pathways initiated by photodynamic therapy. Biochim Biophys Acta 2007;1776:86–107.
[13] Silva JN, Bosca F, Tomé JPC, Silva EMP, Neves MGPMS, Cavaleiro JAS, et al. Tricationic porphyrin conjugates: evidence for chain-structure-dependent relaxation of excited singlet and triplet states. J Phys Chem B 2009; 113:16695–704.
[14] Gaullier JM, Gèze M, Santus R, Sa e Melo T, Mazière J-C, Bazin M, et al. Subcellular localization of and photosensitization by protoporphyrin IX in human keratinocytes and fibroblasts cultivated with 5-aminolevulinic acid. Photochem Photobiol 1995;62:114–22.
[15] Georgiou GN, Ahmet MT, Houlton A, Silver J, Cherry RJ. Measurement of the rate of uptake and subcellular localization of porphyrins in cells using fluorescence digital imaging microscopy. Photochem Photobiol 1994;59:419–22.
[16] Kuimova MK, Yahioglu G, Ogilby PR. Singlet oxygen in a cell: spatially dependent lifetimes and quenching rate constants. J Am Chem Soc 2009;131:332–40.
[17] Reyftmann J-P, Kohen E, Morlière P, Santus R, Kohen C, Mangel WF, et al. A microspectrofluorometric study of porphyrin-photosensitized single living cells. Part I: membrane alterations. Part II: metabolic alterations. Photochem Photobiol 1986;44:461–75.
[18] Klionsky DJ, Abeliovich H, Agostinis P, Agrawal DK, Aliev G, Askew DS, et al. Guidelines for the use and interpretation of assays for monitoring autophagy in higher eukaryotes. Autophagy 2008;4:151–75.
[19] Galluzzi L, Aaronson SA, Abrams J, Alnemri ES, Andrews DW, Baehrecke EH, et al. Guidelines for the use and interpretation of assays for monitoring cell death in higher eukaryotes. Cell Death Diff 2009;16:1093–107.
[20] Viola G, Fortunato E, Cecconet L, Del Giudice L, Dall'Acqua F, Basso G. Central role of mitochondria and p53 in PUVA-induced apoptosis in human keratinocytes cell line NCTC-2544. Toxicol Appl Pharmacol 2008;227:84–96.
[21] Kondo Y, Kanzawa T, Sawaya R, Kondo S. The role of autophagy in cancer development and response to therapy. Nat Rev Cancer 2005;5:726–34.
[22] Xue L, He J, Oleinick NL. Promotion of photodynamic therapy-induced apoptosis by stress kinases. Cell Death Diff 1999;6:855–64.
[23] Kessel D, Vicente MG, Reiners Jr JJ. Initiation of apoptosis and autophagy by photodynamic therapy. Autophagy 2006;2:289–90.
[24] Assefa Z, Vantieghem A, Declercq W, Vandenabeele P, Vandenheede JR, Merlevede W, et al. The activation of the c-Jun N-terminal kinase and p38 mitogen-activated protein kinase signaling pathways protects HeLa cells from apoptosis following photodynamic therapy with hypericin. J Biol Chem 1999;274:8788–96.
[25] Davis RJ. Signal transduction by the JNK group of MAP kinases. Cell 2000;103:239–52.
[26] Ventura JJ, Hubner A, Zhang C, Flavell RA, Shokat KM, Davis RJ. Chemical genetic analysis of the time course of signal transduction by JNK. Mol Cell 2006;21:701–10.
[27] Nakano H, Nakajima A, Sakon-Komazawa S, Piao JH, Xue X, Okumura K. Reactive oxygen species mediate crosstalk between NF-kappaB and JNK. Cell Death Diff 2006;13:730–7.
[28] Shimizu S, Konishi A, Nishida Y, Mizuta T, Nishina H, Yamamoto A, et al. Involvement of JNK in the regulation of autophagic cell death. Oncogene 2010;29:2070–82.
[29] Wei Y, Pattingre S, Sinha S, Bassik M, Levine B. JNK1-mediated phosphorylation of Bcl-2 regulates starvation-induced autophagy. Mol Cell 2008;30:678–88.
[30] Lorin S, Borges A, Ribeiro Dos Santos L, Souquere S, Pierron G, Ryan KM, et al. c-Jun NH2-terminal kinase activation is essential for DRAM-dependent induction of autophagy and apoptosis in 2-methoxyestradiol-treated Ewing sarcoma cells. Cancer Res 2009;69:6924–31.
[31] Lorin S, Pierron G, Ryan KM, Codogno P, Djavaheri-Mergny M. Evidence for the interplay between JNK and p53-DRAM signalling pathways in the regulation of autophagy. Autophagy 2010;6:153–4.
[32] Webber JL, Tooze SA. New insights into the function of Atg9. FEBS Lett 2010;584:1319–26.
[33] Zhang Y, Wu Y, Tashiro S, Onodera S, Ikejima T. Involvement of PKC signal pathways in oridonin-induced autophagy in HeLa cells: a protective mechanism against apoptosis. Biochem Biophys Res Commun 2009;378:273–8.
[34] Cagnol S, Chambard JC. ERK and cell death: mechanisms of ERK-induced cell death—apoptosis, autophagy and senescence. FEBS J 2010;277:2–21.
[35] Wong CH, Iskandar KB, Yadav SK, Hirpara JL, Loh T, Pervaiz S. Simultaneous induction of non-canonical autophagy and apoptosis in cancer cells by ROS-dependent ERK and JNK activation. PLoS One 2010;5:e9996.
[36] Schieke SM, von Montfort C, Buchczyk DP, Timmer A, Grether-Beck S, Krutmann J, et al. Singlet oxygen-induced attenuation of growth factor signaling: possible role of ceramides. Free Radic Res Commun 2004;38:729–37.
[37] Tong Z, Singh G, Rainbow AJ. Sustained activation of the extracellular signal-regulated kinase pathway protects cells from photofrin-mediated photodynamic therapy. Cancer Res 2002;62:5528–35.
[38] Klotz LO, Fritsch C, Briviba K, Tsacmacidis N, Schliess F, Sies H. Activation of JNK and p38 but not ERK MAP kinases in human skin cells by 5-aminolevulinate-photodynamic therapy. Cancer Res 1998;58:4297–300.
[39] Matsubara A, Nakazawa T, Noda K, She H, Connolly E, Young TA, et al. Photodynamic therapy induces caspase-dependent apoptosis in rat CNV model. Invest Ophtalmol Visual Sci 2007;48:4741–7.
[40] Bozkulak O, Wong S, Luna M, Ferrario A, Rucker N, Gulsoy M, et al. Multiple components of photodynamic therapy can phosphorylate Akt. Photochem Photobiol 2007;83:1029–33.
[41] Sebolt-Leopold JS, Herrera R. Targeting the mitogen-activated protein kinase cascade to treat cancer. Nat Rev Cancer 2004;4:937–47.
[42] Cheng JQ, Lindsley CW, Cheng GZ, Yang H, Nicosia SV. The Akt/PKB pathway: molecular target for cancer drug discovery. Oncogene 2005;24:7482–92.